applied sciences

MDPI

Review

Synchrotron FTIR Microspectroscopy Investigations on Biochemical Changes Occurring in Human Cells Exposed to Proton Beams

Ines Delfino [1], Valerio Ricciardi [2] and Maria Lepore [3,*]

[1] Dipartimento di Scienze Ecologiche e Biologiche, Università della Tuscia, I-01100 Viterbo, Italy; delfino@unitus.it
[2] Istituto Nazionale di Fisica Nucleare—Sezione di Napoli, I-80126 Napoli, Italy; vricciardi@na.infn.it
[3] Dipartimento di Medicina Sperimentale, Università della Campania "Luigi Vanvitelli", I-80138 Napoli, Italy
* Correspondence: maria.lepore@unicampania.it; Tel.: +39-081-5665839

Abstract: Fourier transform infrared microspectroscopy using a synchrotron radiation source (SR-μFTIR) has great potential in the study of the ionizing radiation effects of human cells by analyzing the biochemical changes occurring in cell components. SR-μFTIR spectroscopy has been usefully employed in recent years in some seminal work devoted to shedding light on processes occurring in cells treated by hadron therapy, that is, radiotherapy with charged heavy particles (mainly protons and carbon ions), which is gaining popularity as a cancer treatment modality. These studies are particularly useful for increasing the effectiveness of radiotherapy cancer treatments with charged particles that can offer significant progress in the treatment of deep-seated and/or radioresistant tumors. In this paper, we present a concise revision of these studies together with the basic principles of μFTIR spectroscopy and a brief presentation of the main characteristics of infrared SR sources. From the analysis of the literature regarding the SR-μFTIR spectroscopy investigation on human cells exposed to proton beams, it is clearly shown that changes in DNA, protein, and lipid cell components are evident. In addition, this review points out that the potential offered by SR-μFTIR in investigating the effects induced by charged particle irradiation have not been completely explored. This is a crucial point for the continued improvement of hadron therapy strategies.

Keywords: Fourier transform infrared microspectroscopy; infrared synchrotron radiation; human cells; proton irradiation; hadron therapy

Citation: Delfino, I.; Ricciardi, V.; Lepore, M. Synchrotron FTIR Microspectroscopy Investigations on Biochemical Changes Occurring in Human Cells Exposed to Proton Beams. *Appl. Sci.* **2022**, *12*, 336. https://doi.org/10.3390/app12010336

Academic Editor: Itzhak Orion

Received: 21 November 2021
Accepted: 24 December 2021
Published: 30 December 2021

1. Introduction

Fourier transform infrared (FTIR) spectroscopy measures vibrational energy levels related to chemical bonds. This technique allows one to acquire spectra that are considered as a fingerprint of the investigated samples. In particular, FTIR spectroscopy measures the light absorption by specific molecules using a broadband light source. FTIR spectrometers equipped with microscope stages (μFTIR spectroscopy) have been used in an extremely large number of fundamental and applied biomedical research fields due to the high sensitivity of revealing detailed information on molecular composition, structure, and interactions with non-destructive sampling and reduced analysis time in comparison to other conventional methodologies [1–3].

The performances of μFTIR spectroscopy are substantially improved using synchrotron infrared radiation sources. Since the 1980s, there has been a growing interest in the use of these sources due to the fact of their high brilliance, which allows for the improvement of the spatial resolution up to the diffraction limit. This enables the acquisition of high-quality single cell spectra even in an aqueous environment [4–6]. These characteristics have been largely exploited for investigating cellular systems in different experimental conditions [7–12].

μFTIR spectroscopy has also been demonstrated to be a useful tool in radiobiology, since it can rapidly and non-invasively investigate the complex biological processes occurring in cells exposed to ionizing radiation, such as proliferation and cell death processes, and it has attracted a growing interest in the field of radiation-induced cyto- and genotoxicity [13–19]. In addition, in this field, μFTIR spectroscopy has benefited from the use of SR sources managing to study single cells in an aqueous environment [16,20–23].

Over the last years, hadron therapy that uses charged particles, as protons and carbon ions, has acquired a noticeable importance in radiotherapy treatment due to the several advantages that charged particles give in comparison to photons [24,25]. Charged particles release most of their energy at the end of their range; thus, they offer a much better localization of the dose distribution within the tumor volume in comparison to X-rays. In this way, the transfer of very high-dose gradients close to organs at risk is allowed, and the high-dose area is confined to the tumor volume. However, significant improvement in hadron therapy outcomes is strictly related to the possibility of obtaining fast and accurate information on cell response. For this purpose, some researchers recognized the potential of SR sources and μFTIR spectroscopy for enlightening the complex processes occurring after cell exposure to proton beams.

In this paper, we aimed at presenting a concise review of these studies together with the basic principles of μFTIR spectroscopy and a brief presentation of the principal characteristics of infrared radiation synchrotron sources.

2. FTIR Microspectroscopy

FTIR spectroscopy is based on the spectral analysis of the IR radiation absorbed by a sample. The energy of radiation absorbed is equal to the energy to be provided for inducing a transition between two vibrational states of a specific functional group present in the sample. This means that the contributions from different biochemical bonds present in a sample originate the IR absorption spectrum, which comprises several peaks or bands, each referred to a particular mode of vibration characteristic of functional groups in the sample [1,2]. FTIR is an advanced and powerful optical technique for obtaining absorption spectra in the infrared region from various kinds of samples and thus getting qualitative information on the structure of the analyzed substances. Quantitative data about the compounds can be obtained, too, also thanks to the use of modern computational algorithms.

In FTIR spectroscopy, high-resolution spectra are collected simultaneously over a wide spectral range. This confers a significant advantage over traditional IR absorption spectroscopy, which enables the detection of spectral data over a narrow range of energies at a time. On the contrary, using FTIR spectroscopy, all the frequencies are simultaneously analyzed and registered by the detector. FTIR spectroscopy offers other practical advantages compared to traditional IR, such as a lower energy dispersion, high precision, and accuracy, in the discrimination of wavelengths with the possibility to superimpose the monochromatic radiation of a laser source as an internal standard and the possibility to obtain spectra from a very wide range of samples at any temperature (the source is sufficiently far from the sample and, therefore, there is no heating effect) and pressure with appropriate devices and accessories.

The main component of an FTIR system is Michelson's interferometer (Figure 1), which replaces the monochromator usually employed in traditional IR spectrometers. Thanks to the use of the interferometer, each wavelength of the light beam is periodically blocked and transmitted due to the fact of wave interference. The interferometer consists of three mirrors: A fixed mirror and a moving one forming an angle of 90° with the first mirror. The third mirror (called a "beam splitter" mirror) is placed at an angle of 45° with respect to the incident light. The beam coming from the source arrives on this splitter, which collimates and divides it into two perpendicular rays of equal intensity (see Figure 1).

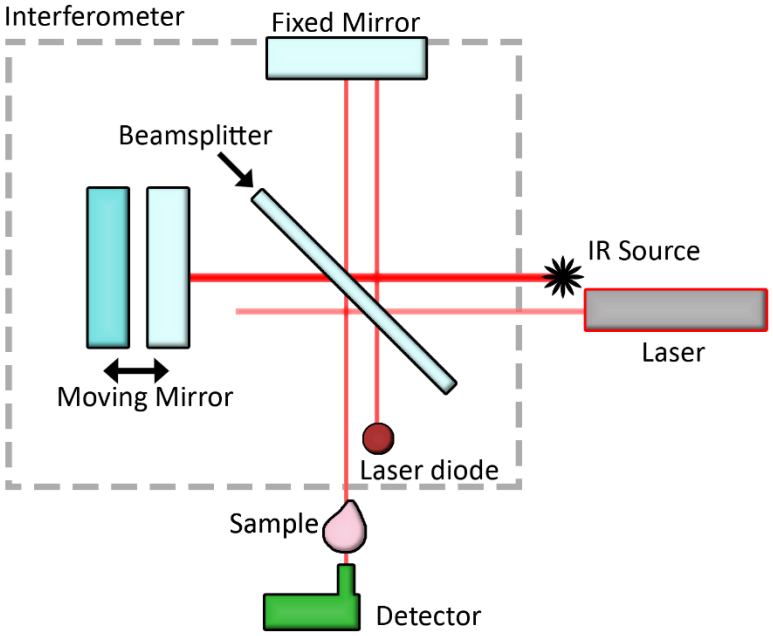

Figure 1. Scheme of a Fourier transform infrared spectrometer.

One of these two rays is reflected along a path directed to the fixed mirror, and the other goes through the splitter and is then transmitted to the moving mirror. The first ray is reflected by the fixed mirror and arrives again on the splitter. From the splitter, the light is partially sent back to the source and partially transmitted and focused on the detector. The third mirror moved forward parallel to itself along the other branch of the interferometer path and reflects the other ray on the splitter from different distances. This ray is then partially returned to the source and partly reflected towards the detector, where an intensity given by the algebraic sum of the intensities of the two rays is detected and represented as an interferogram. These data are treated by the instrument through the Fourier transform algorithm to obtain the traditional absorption spectrum.

The sample to be investigated is placed between the two arms of the interferometer. The FTIR spectroscopy apparatus can be equipped with a microscope to allow the microscopic analysis of samples or parts of samples up to one micron in size.

In Figure 2 of Reference [26], typical SR-μFTIR spectra of cells exposed to proton beams are reported. It was obtained for living prostate cancer PC-3 cells. The spectral features are reported in dependence of the wavenumber (defined as the number of wavelengths per unit distance) expressed in cm^{-1}. This is the way the information about the energy is usually given in IR absorption spectroscopy instead of using frequencies or wavelengths (see Figure 2 in the present paper). In the spectra, different contributions from lipids, proteins, and nucleic acids are clearly visible. For identifying these different contributions, deconvolution procedures are usually performed. This analysis consists in writing the complex spectra as a sum of Gaussian–Lorentzian-shaped vibrational modes. Detailed information about the modes was obtained by a nonlinear fitting procedure which had starting conditions (i.e., the starting values of the parameters of the single modes) that were obtained by manual selection. The procedure allows for the determination of the optimized intensity, position, and width of the peaks by using the χ^2 parameter for controlling deconvolution procedure performances [19]. This procedure can also be used for monitoring the changes in the peak position due to the interaction with ionizing radiation [19].

In Figure 2, the results of this analysis performed on IR spectra from normal human MCF-10A breast cells are shown, and in Table 1, the assignments for the different functional groups are reported. The region at approximately 2950–2850 cm^{-1} is related to the lipid and protein contributions, the absorption bands in the range at approximately 1750–1500 cm^{-1} and in the region 1490–1250 cm^{-1} are attributed to protein components, while the features

in the 1230–1000 cm^{-1} range are ascribed to DNA/RNA contributions. From Table 1, it can be noticed that the region at longer wavenumbers (i.e., 3000–3400 cm^{-1}) can also offer information on proteins [27].

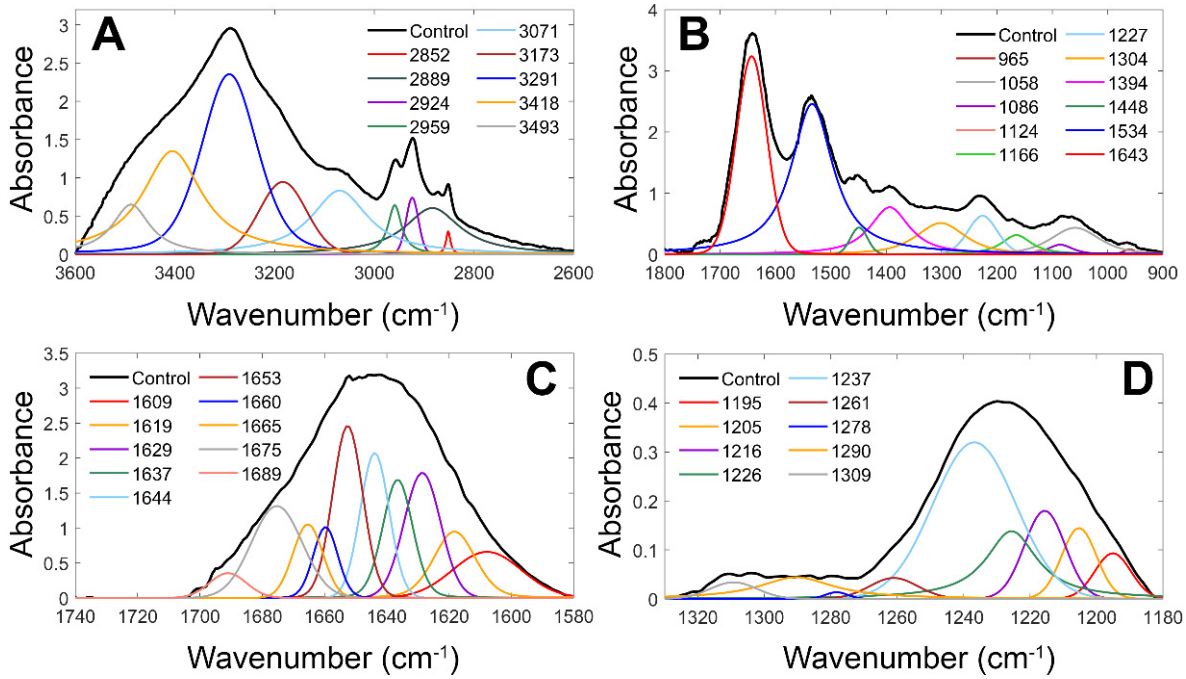

Figure 2. Deconvolution of a μFTIR spectrum acquired from normal human MCF-10A breast cells in the different spectral regions. In the (**A** panel) the high wavenumber region (3600–2600 cm^{-1}) is shown, in the (**B** panel) the same is shown for the fingerprint region (1800–900 cm^{-1}), in the (**C** panel) the same is shown for the Amide I band region (1740–1580 cm^{-1}), and in (**D** panel) the same is shown for the Amide III band region (1350–1180 cm^{-1}). Reprinted from Reference [19] under open access conditions.

Table 1. FTIR peaks observed in the spectrum of MCF-10A breast cells, with assignments in agreement with the data reported in the literature (see Reference [19] and references therein); as = asymmetric, s = symmetric, ν = stretching, δ = bending, sc = scissoring, vbr = vibration, a. a. = free amino acids. The indicated position of every peak is the center of the relative Gauss-cross-Lorentzian function obtained from the deconvolution fit.

Peak (cm^{-1})	Assignment			
	DNA/RNA	**Protein**	**Lipid**	**Carbohydrate**
3500–3300				O–H ν
3291		Amide A (–N–H ν)		
3173		$–NH_3^+$ as. N (a. a.)		
3071		Amide B (–N–H ν, δ)		O–H ν
2959		CH_3 as. ν	CH_3 as. ν	
2924			CH_2 as. ν	
2889		CH_3 s. ν	CH_3 s. ν	
2852			CH_2 s. ν	
1643		Amide I (C=O ν, C–N ν)		
1534		Amide II (C–N ν, C–NH δ)		
1448		CH_3 as. δ, CH_2 sc.	CH_3 as. δ, CH_2 sc.	
1394		COO^- s. ν		
1304		Amide III (–N–H δ, C–N ν)		

Table 1. *Cont.*

Peak (cm^{-1})	Assignment			
	DNA/RNA	**Protein**	**Lipid**	**Carbohydrate**
1291		Amide III (–N–H δ, C–N ν)		
1227	PO_2^- as. ν	C–O–P ν		
1207	C–H ring δ			
1171	Sugar-phosphate backbone vbr.			
1166			CO–O–C s. as. ν	
1143	Ribose C–O ν			
1124	C–O ν			
1100	P–O–C s. ν			
1086	PO_2^- s. ν		C–O–P ν	
1058	C–O ν			
965	PO_4^- s. ν		C–O ν, C=C ν (a. a.)	

3. IR Synchrotron Radiation Sources and FTIR Spectroscopy Techniques

The first X-ray experiments with synchrotron radiation were performed in the 1960s, while the first developments of the synchrotron radiation in the IR region were obtained in the 1970s, and the first facility for the use of infrared synchrotron radiation (IR-SR) was established at Daresbury at the beginning of the 1980s [2]. Later, many other beamlines dedicated to infrared SR were established, and SR-μFTIR applications nowadays span from solid-state physics, gas-phase studies, surface science, earth and planetary science, archaeology to life sciences, biomedicine, biophysics, nano spectroscopy, and imaging [5,6].

Bending magnets are generally adopted for developing an IR-SR source that exploits the emission from the dipole magnets that curve the electron beam into a closed trajectory. Since SR in the infrared wavelength range is characterized by a large size and intrinsic divergence of the beam, it is necessary to use suitably sized optics for transferring and focusing the infrared beam from the large exit port of the storage ring to the entrance of the associated spectrometer. The first optical component of an infrared beamline is a flat mirror that is adopted for deviating the emitted photon out of the bending magnet region to another flat or focusing mirror. The first mirror is named the extraction mirror, which constitutes a very important element of the beamline. Particular care is required for its positioning and shaping. In Reference [6], details on the optical setups used for infrared beam propagation control are reported. The principal advantage in using an IR-SR for spectroscopy is related to its very high brilliance. This physical parameter is defined as the number of photons per unit of time(s) per 0.1% of bandwidth and the results of at least two orders of magnitude greater than a thermal source. In Figure 3, the comparison between the calculated IR-SR brilliance of a 3 GeV SR source and a Globar thermal source is reported.

The high brilliance is extremely useful for obtaining high-quality spectra from heterogeneous and complex samples. In addition, IR-SR is strongly polarized, pulsed, and characterized by a broadband emission. It is important to note that some laser sources have similar characteristics as far as concerns brightness, but the IR-SR source is the only one with a broadband emission covering the entire infrared wavelength range (from far-IR (i.e., 250–300 μm) to near-IR (i.e., 0.7–1 μm)) [28].

As said before, FTIR experiments require the use of a spectrometer system. Commercial Fourier transform infrared microspectrometers can be used with IR-SR sources, and the operation modalities are the same as for thermal sources. Array detectors, known as focal plane arrays (FPAs), are generally used, since they offer the advantage of reducing the acquisition time [29].

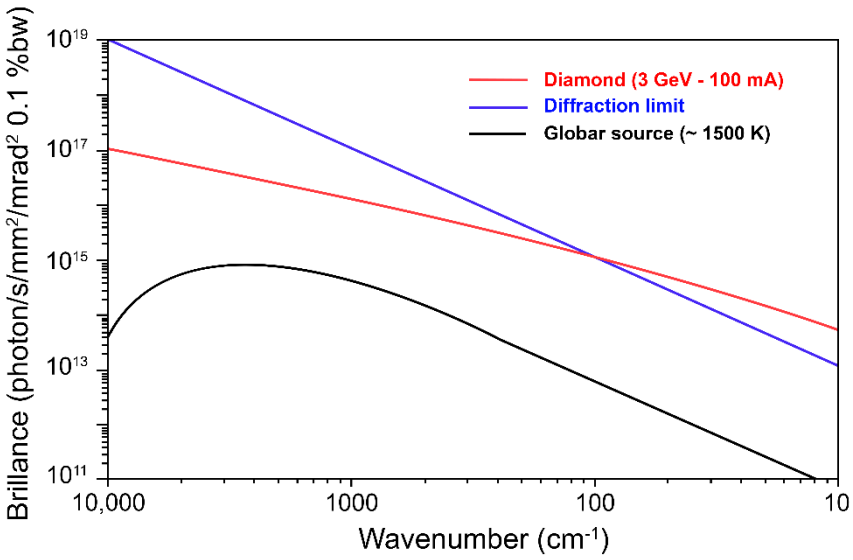

Figure 3. Comparison of the calculated SR brilliance of a 3 GeV SR source (red), a Globar (black), and an ideal bending magnet SR diffraction limited source (blue). Reprinted with permission from Reference [5].

Microspectrometer systems benefit from the high brilliance of the IR-SR sources that allow for the reduction in the aperture slits of an IR microscope and for the collection of data in the mid-IR region with a good signal-to-noise ratio from geometrical areas of a few microns (at the diffraction limit [30]). Consequently, the main advantage of FTIR microscopy when using an IR-SR source is the possibility to achieve the highest spatial resolution at the sample location, i.e., at the micron scale. This allows for a true single-cell analysis that is of paramount importance in many biomedical applications. The high brilliance of IR-SR sources not only allows for the study of single cells but also permits to have them in an aqueous environment, i.e., in living conditions [31]. In fact, the strong absorption of water in the mid-infrared region has for a long time required the dehydration of samples as a necessary step to acquire high-quality spectra, but the use of IR-SR sources together with properly designed sample holders and efficient subtraction algorithms has made it possible to adopt infrared spectroscopy for investigating samples in an aqueous environment [11,20–23].

4. Rationale of Proton Beam Therapy

Although at the time of diagnosis, about 50% of cancers have not yet metastasized, cancer remains a major cause of death nowadays [32,33]. In cases where it is possible to intervene clinically, tumours can be treated with therapies as surgery, chemotherapy, and radiotherapy, often used in combination; despite this, in only 80% of cases, medical treatments are successful in completely removing the tumours or inactivating them [34]. Hadron therapy is an increasingly diffused radiation treatment modality that uses beams of accelerated charged particles as a tool for tumours treatments [35]. Conventional radiotherapy, which uses high-energy photons, is mainly useful for the treatment of superficial tumours due to the release of energy in matter with an exponentially decreasing trend with depth [36]. Furthermore, at equal doses, photons are radiobiologically less effective than particle beams, especially those heavy as carbon ones. The greater ballistic accuracy in the dose delivered to the tumour volume and the higher radiobiological effectiveness, considering the carbon ions, are the main clinically relevant advantages of hadron therapy in respect of the conventional radiotherapy. The first property is directly related to the type of energy deposition along and around the path of ion beams in the matter, described by the well-known Bragg curve. It results in a greater sparing of normal tissue and/or organs at risk compared to photons. The second propriety, on the other hand, depends on the different response of the tumour cells to ionizing radiations of different quality; in general

term, in fact, the biological effectiveness, that is, the ability to suppress more cells at an equal amount of dose, increases as the number Z of the particles used increase.

Indeed, significant progress in the treatment of deep-seated and/or radioresistant tumours have been achieved using mainly protons and carbon ions particle therapy. The possible use of beams with lower or higher atomic number (Z) particles, such as helium, lithium or oxygen, [37], in the clinic, is currently a main subject of study.

When charged particles interact with matter, the continuum of the ionization events produced by ions (the track structure) is related to the particles' energy, and for a given energy, to Z. It is important to evidence that even at equal/similar linear energy transfer (LET) values (a parameter used to describe the local energy deposition from particles in the matter), particles with different Z can cause qualitatively and quantitatively different biological effects owing to secondary ionization events, consequently to their track structure. For these reasons, it would be useful to evaluate the damage level along the whole path of the charged particle beam in order to determine the relative biological effectiveness (RBE) changes along the entire Bragg curve. Obviously, experimental studies are mainly concentrated into the spread-out Bragg peak (SOBP) region (Figure 4), which can be seen as a "broadened" peak that is obtained, during therapies, as a convolution of multiple mono-energetic Bragg curves, modulating the particle beam energy to uniformly contour the tumoral region. The main physical motivation of the use of hadrons in tumour therapy is the high value obtainable for the ratio between the energy deposited in the SOBP and the one delivered at the beam entrance/plateau region, which can reach the order of two or even three for carbon ions. A criticality is represented by the fact that most of the existing data focus on the radiobiological effects only in the SOBP region, and therefore in the tumour area, while there is still relatively little knowledge on the sub-lethal effects on healthy tissue related to the remaining areas of the Bragg profile, such as the plateau region and the region immediately behind the SOBP, with the second being of particular relevance for carbon ion hadron therapy due to beam fragmentation process occurring after the passage in the tumoral region [38]. The dose released to healthy tissues is a source of sub-lethal damage that, if poorly repaired and inherited by the progeny, can lead to the formation of chromosomal alterations which are, in turn, potentially carcinogenic [36,39–42].

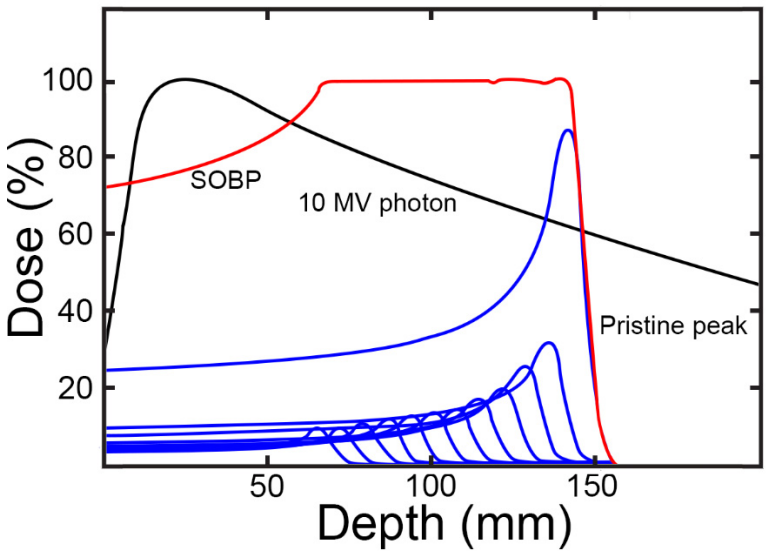

Figure 4. Distribution of dose percentage in respect of penetration depth for a spread-out Bragg peak of a particle beam (red line). The SOBP dose distribution is the result of the convolution of different mono-energetic Bragg peaks (blue lines). The depth–dose distributions of a 10 MV photon beam (black line) is reported for confrontation.

More detailed biophysical models on the effects of high LET radiation along the entire widened Bragg curve are therefore necessary.

The few studies conducted for this purpose show that there is a relevant change in the radiation-induced damage along the Bragg curve, depending on the choice of the ion, on the dose and the examined endpoint (aberrations, micronuclei, senescence, etc.) [43]. As said before, it is decisive to know what biological effects are induced, in the region behind the SOBP, especially for heavy ions, for which a "tail" in the dose delivered exists, which is due to the fragmentation of the projectiles in the incident beam. Secondary ions with a lower Z value and less energy (hence with a higher LET) will be produced, and they will stop in the healthy tissue, contributing to the total dose released from the primary beam itself.

5. The Contribution of the SR-μFTIR Spectroscopy to the Characterization of Proton Irradiated Cells

The enormous potentialities of SR-μFTIR spectroscopy in examining cell samples exposed to different external agents have been largely exploited in various experimental conditions [6–12].

As said before, a limited number of researchers has adopted SR-μFTIR spectroscopy for characterizing the effects of proton beam exposure on different human cell lines. A preliminary characterization of proton-induced effects by means of μFTIR spectroscopy was reported for single PC-3 cells using a commercial system with a conventional infrared source [44]. For proton treatment, cells were seeded on 35 mm diameter Petri dishes with 10 mm round holes. The bottom of the Petri dish was capped with a 1.5 μm thick Mylar foil. About 10,000 cells in 10 μL medium were seeded in the central part of the Mylar foil 16–18 h before the experiments. When cells had adhered to the foil (4 h after the seeding), 2 mL of medium was added. A 2 MeV focused proton microbeam extracted from the Van de Graaff accelerator was used for irradiating cells with four doses of protons in the range of 1000–8000 protons per cell and next incubated with the medium at 37 °C and an atmosphere of 5% CO_2 for up to 24 h. After, all cells were washed with PBS and fixed in 70% ethanol at 4 °C. The experimental control group consisted of non-irradiated cells, processed in the same way.

Spectra were collected in transmission mode with a resolution of 4 cm^{-1}, in the spectral range of 600–4000 cm^{-1} for all groups of cells. After pre-processing analysis (see Reference [45] for details), the spectra were analyzed using the abovementioned deconvolution procedure by fitting the spectra with a sum of Gaussian–Lorentzian curves (see Figure 2 of Reference [44]). Band fitting was performed in the spectral region of 800–1800 cm^{-1}, because the authors were interested in the detection of changes in the DNA backbone spectral range (950–1240 cm^{-1}). The results of the band fitting procedure were similar to the ones reported in Table 1 of the present paper (see Table 2 of Reference [44] for further details). All modifications observed in the spectra of cells irradiated by 1000 and 2000 protons per cell were not statistically significant. Instead, changes observed when higher doses were used were significant, with those observed after 8000 protons-per-cell irradiation being higher than those observed after 4000 protons-per-cell irradiation. The area of the O–P–O symmetric stretching band increased with the number of protons, while the area of the P–O–C symmetric stretching band decreased with the number of protons. It could mean that the probability of DNA strand breaks by destroying the C–O bond is higher than the O–P one. An increase with the number of protons in the area under the band corresponding to the motion bond in phosphate–DNA backbones may be ascribed to the destroyed chromosomal structure. Fragmentation of chromosomes could cause an increase in the number of molecule freedom degrees. The emergence of a new peak at approximately 830 cm^{-1} in the spectra of cells irradiated with 8000 protons per cell was observed. Simulations show that this peak could be correlated with single-stranded breaks [44].

The PC3 cells exposed to proton beams were also investigated using SR-μFTIR spectroscopy, and the spectral region related to nucleic acids, proteins, and lipids were analyzed separately [46]. In this case, cells were irradiated with protons and examined with μFTIR spectroscopy using the same support for minimizing the loss of treated cells. The substrate

had to be transparent for both protons and infrared radiation. To this purpose, silicon nitride membranes were used, and cells were irradiated with 50–4000 protons (corresponding to energy ranging from 3.2 to 260 MeV). Treated and untreated cells were washed in PBS and then fixed in 3.7% paraformaldehyde (20 °C, 10 min) immediately or 24 h after irradiation. The early fixed cell can allow for the study of DNA damage, while the later fixed cells enable for the investigation of the cellular response and repairing mechanisms.

The SR-μFTIR spectra were acquired in the transmission mode at the IRENI beamline (SRC, University of Wisconsin-Madison) [47]. An FTIR Vertex 70 spectrometer equipped with a Hyperion FTIR microscope with a focal plane array 64 × 64 element detector was used. The SR-FTIR images were collected using a 74× objective (Ealing Inc., Rocklin, CA, USA). One hundred and twenty-eight scans were co-added for obtaining a good signal-to-noise ratio.

In order to detect DNA damage, infrared spectra from cells fixed immediately after proton irradiation were examined using a second derivative and principal component analysis (PCA).

Derivative analysis and PCA are two approaches largely used in the analysis of infrared spectra. By inspecting first or higher derivatives of absorbance with respect to wavelength, qualitative and quantitative information are obtained from infrared spectra. The technique was first introduced in the 1950s, and it is useful for more specific identification of small and nearby lying absorption peaks which are not well-resolved in the original spectrum, thus improving the specificity of absorption peaks. Another important advantage in the use of the second derivatives is that constant and linear components of baseline errors are removed. In the beginning, this technique did not receive much attention due to the complexity of generating derivative spectra. The availability of modern calculation tools allows for the use of mathematical methods to generate derivative spectra quickly, easily, and reproducibly. This significantly increased the use of the derivative technique (see [48,49] for further details).

PCA has been proven to be especially effective for analyzing infrared spectra, too. It is based on a mathematical decomposition of the spectral data with the aim of reducing data set dimensions by using only some new principal components (PCs) or loadings that explain most data set variance and then are thought to carry the most important information of the spectra [50]. Spectral data can be inspected by using different combinations of PCs to obtain a new system of coordinates. PCA is based on the analysis of the correlation or covariance matrix. The number of components necessary to explain at least 80% of the total variance is usually considered. Recently, selected regions of Raman spectra have been separately analyzed by PCA to extract information hidden in those specific ranges. This kind of approach is called the interval-PCA (iPCA) method [51].

An example of the results that can be obtained by PCA in this framework is reported in Reference [46]. In this case, the second derivatives analysis reported in Figure 2B of Reference [46] indicated an intensity change of the O–P–O symmetric stretching mode at 1083 cm^{-1}. The decrease in intensity shows a dose-dependent behavior that can indicate the occurrence of strand cleavage and chromatin fragmentation [52,53]. This last effect is due to the high number of DSBs. The small shift of the O–P–O asymmetric stretching band at approximately 1234 cm^{-1} was probably caused by local conformational changes in the DNA.

PCA was applied to different groups of infrared spectra collected from cells fixed immediately after irradiation. In the first case, four groups of cells were considered: (a) irradiated by 4000 protons; (b) irradiated by 200 and 400 protons; (c) irradiated by 50 protons; (d) the untreated ones. PCA showed that PC-1 (corresponding to 73% of the total variance) was positively correlated with features attributed to vibrations of DNA base-sugar bonds C–O–P furanose–DNA backbone stretching vibrations and O–P–O symmetric and asymmetric stretching in DNA. In the second case, PCA was applied to two groups of spectra acquired from control cells and cells irradiated with 4000 protons per cell and fixed just after irradiation. In this case, a very good separation of controls versus irradiated cells

on the PC1 versus PC2 scores plot was evidenced for the two groups (see Reference [46] and Figure 4a,b therein for further details).

To study the cellular response and the repairing processes after exposure to ionizing radiation, the spectra acquired from cells fixed 24 h after irradiation were examined. In this case, lipid accumulation was evidenced by an increase in the lipid ester carbonyl mode and other CH lipid bands. These variations were discussed as related to an increase in lipid metabolism during apoptosis and the inclusion of lipid droplets involved in the formation of apoptotic bodies. The lipid peroxidation effect was considered as the cause of the observed decreased intensity of the CH_3 stretching mode and the increased intensity of the CH_2 stretching mode [46].

The same group of researchers also investigated prostate cancer cells derived from brain metastasis (DU-145 cell line) using two experimental setups for μFTIR spectroscopy. The former uses a Globar source with a focal plane array (FPA) detector and the latter a synchrotron radiation source with a mercury–cadmium–telluride (MCT) detector [54]. The high brightness of the SR source allowed for the acquisition of spectra from individual cells and permitted them to study the contribution of DNA in the spectral region 1300–900 cm^{-1}, which is usually difficult for conventional μFTIR spectroscopy due to the high density of the nucleus.

For proton irradiation, DU-145 cells were treated as previously described for the PC-3 cells. In this case, cells were irradiated using a 1 MeV focused proton microbeam from the van de Graaff accelerator, which available at the Institute of Nuclear Physics PAN, Krakow, Poland. The DU-145 cells were placed on Mylar foil, as were the PC3-cells, approximately 16–18 h before the irradiation treatment and were irradiated with the counted number of protons (50, 200, 400, 2000, and 4000 protons per cell). In addition, in this case, cells were fixed in 70% ethanol at 4 °C.

Spectra were collected using the two abovementioned μFTIR spectroscopic setups. All measurements were performed at the SISSI beamline, ELETTRA Laboratory, Trieste, Italy. A Bruker Vertex 70 coupled with the Vis/IR HYPERION 3000 microscope. The SR-FTIR spectra were acquired in the transmission mode with a spectral resolution of 4 cm^{-1} in the 4000–600 cm^{-1} wavenumber region. For each spectrum, 512 scans were co-added to reach a good signal-to-noise ratio. An aperture of 12 × 12 μm was used for collecting single-cell spectra. The FTIR images were also obtained using a Globar and FPA detector with 15× Cassegrain objective in the transmission mode in the 4000–950 cm^{-1} wavenumber region. For each spectrum, 64 scans were added with the same spectral resolution of SR-FTIR.

In Reference [54], the authors focused their attention on the spectral ranges related to the contributions of various cell components. Preliminarily, they examined the phosphodiester symmetric stretching region (i.e., 1130–900 cm^{-1}) and the CH_2/CH_3 stretching spectral range (i.e., 3000–2800 cm^{-1}) using both FTIR apparatus. The two apparatus gave similar results, but the absorption of the Mylar foil on which the cells were seeded altered the spectral trend in the phosphodiester asymmetric stretching region. A dose dependence was observed for all the spectra as evidenced by the second derivatives' approach (see Figures 2 and 3 in Reference [54]).

Changes in DNA were evidenced at 970 cm^{-1} due to the deoxyribose–phosphate skeletal motions (C–C) especially for the 2000 and 4000 proton doses. The authors attributed this effect to SSB, DSB, crosslinks, and deoxyribose damage in agreement with References [53,55]. Differences were also present for the O–P–O symmetric stretching mode at 1090–1080 cm^{-1} and the C–O furanose stretching vibrations at 1020 and 1060 cm^{-1}. Since furanose is a relevant biomarker for base-pairing and base-stacking in RNA, the authors suggest that changes in RNA molecules due to the proton exposure could cause the occurrence of improper translation processes. The analysis of the 3000–2800 cm^{-1} spectral region, in which CH_2 and CH_3 symmetric and asymmetric stretching modes features were present, indicated changes in intensity that can be related to phospholipid membrane compaction following peroxidation [54].

The phosphodiester (i.e., 1130–950 cm^{-1}) and the phospholipid (i.e., 3000–2800 cm^{-1}) regions were also examined by using PCA of the second derivatives. The resulting scores and loading plots for the SR-FTIR and Globar IR source were quite similar. This analysis indicated that the modifications induced in the cellular spectra by proton irradiation were reproducible, and for both experimental approaches, PCA could individuate six cell groups (i.e., the control and the five irradiated groups of cells). In Reference [54], a detailed description of the results of the PCA can be found. The most relevant result is related to the dose-dependent changes in the relative intensities of the DNA peak at 970 cm^{-1} and the shift of O–P–O that can be correlated to DNA damage (single- or double-stranded breaks).

The effects of proton exposure were also investigated in A-172 glioblastoma cells [56]. In this study, the authors focused their attention on the spectral changes occurring in single cellular nuclei isolated from cells treated with protons. In this paper, AFM-IR (atomic force microscopy-IR) measurements were also performed for taking advantage of the increased spatial resolution offered by this approach. Cells were treated with 1 and 10 Gy of protons at the Institute of Nuclear Physics PAN in Krakow (Poland) after an incubation time of 24 and 48 h cellular nuclei were extracted.

A drop of nuclei in saline solution was placed between two CaF_2 windows. Infrared spectra of single cellular nuclei in saline solution were acquired at the infrared microspectroscopy beamline at the ANSTO Australian Synchrotron in Clayton (Australia) using a Bruker V80 FTIR and HYPERION microscope equipped with a narrow band MCT detector. An aperture of 10 $\times$ 10 μm was set. Spectra acquisition was performed in the transmission mode in the 4000−750 cm^{-1} wavenumber range with a spectral resolution of 4 cm^{-1}.

Second derivative analysis and PCA were used for analyzing the acquired spectra. The spectral features of isolated nuclei and cells were analogous, but the DNA bands were more evident in nuclei spectra. This result could be due to the higher sensitivity of cell nuclei to radiation exposure than that of cytoplasm. The authors focused their attention on the peak located at 1230 cm^{-1} due to the O−P−O asymmetric stretching mode from the DNA, the band at 1660 cm^{-1} attributed to the Amide I band, and the features observed at 2952 cm^{-1} resulting from asymmetric stretching of methyl groups from lipid contribution. The analysis of SR-μFTIR spectra evidenced that exposure to 10 Gy of protons causes a strong increase in the lipid content with the presence of principally cholesterol and cholesteryl esters. Spectral modifications related to DNA damage and repairing processes were also evident. The decrease in the intensity of the 1713 cm^{-1} feature can be attributed to the base-pair damage including purine, pyrimidine dimer formation, and lesions, and it was observed in the spectra from nuclei isolated from cells treated by 1 and 10 Gy of protons. Radiation exposure also caused a shift in the O−P−O asymmetric stretching band towards a lower wavenumber value, indicating the occurrence of DNA conformational changes. This shift from 1220 to 1240 cm^{-1} was present in the SR-μFTIR spectra of nuclei exposed to 10 Gy of protons and extracted after 48 h of incubation. The decrease in the intensity of this peak can be related to the experimental evidence that after radiation exposure, the cells were stopped in the G1 phase during DNA repairing processes. Cells in the G1 phase are characterized by a smaller band related to phosphodiester bonds. Exposure to 10 Gy of protons can be also associated with an increase in the intensity of the Amide II band at 1550 cm^{-1} in SR-μFTIR spectra collected from nuclei extracted from cells 24 and 48 h after irradiation. This change can be related to the enzymes involved in DNA repair (see Figures S2–S4 in the Supplementary Materials of Reference [56], freely available, and Reference [19]) and to sterol synthesis processes in cells irradiated with protons.

PCA was performed in two wavenumber regions (i.e., 1800–1030 and 3000–2750 cm^{-1}), and the Amide I spectral range was not included in the analysis because of the presence of water contribution due to the saline solution used during the spectra acquisition. Results confirmed the lipid accumulation (mainly cholesterol and cholesteryl esters) in cancer cells. This represents a biomarker for aggressive cancer cells that produce membranes for rapid cell proliferation. In addition, lipids play an important role in cancer cell migration and

invasion processes that are of relevant importance in the distribution of tumor cells and the formation of metastases [56].

6. Conclusions

In this short review, we briefly described μFTIR principles of operation and the advantages offered by IR-SR to this vibrational spectroscopic technique. We focused our attention on a certain number of investigations that used SR-μFTIR and advanced data analysis procedures for studying the changes induced by proton irradiation on various human cell lines. The use of IR-SR sources allows for the conduction of single-cell investigations to study DNA damage and repair mechanisms occurring after proton exposure. Measurements evidenced changes not only in DNA but also in protein and lipid cell components. Modifications in DNA have been correlated to single- or double-stranded breaks, while changes in proteins have been associated to the enzymes involved in DNA repair. In addition, alterations in lipid features have been proved to take place in tumor cells. The results revised here suggest that the use of SR-μFTIR spectroscopy together with sophisticated analysis procedures can offer a valid tool to improve knowledge of the effects induced by proton beam exposure, opening the possibility of personalized hadron therapy treatment. For this reason, it would be desirable to extend SR-μFTIR spectroscopy to a greater number of cell systems treated under well-controlled conditions and examined at single-cell levels also in an aqueous environment to expand our knowledge on cell–proton interaction in conditions closer to physiological ones.

Author Contributions: Conceptualization, I.D. and M.L.; methodology, I.D. and M.L.; formal analysis, I.D., V.R. and M.L.; writing—original draft preparation, I.D., V.R. and M.L.; writing—review and editing, I.D. and M.L.; supervision, M.L. All authors have read and agreed to the published version of the manuscript.

Funding: This research received no external funding.

Institutional Review Board Statement: Not applicable.

Informed Consent Statement: Not applicable.

Conflicts of Interest: The authors declare no conflict of interest.

References

1. Baker, M.J.; Trevisan, J.; Bassan, P.; Bhargava, R.; Butler, H.J.; Dorling, K.M.; Fielden, P.R.; Fogarty, S.W.; Fullwood, N.J.; Heys, K.A.; et al. Using Fourier transform IR spectroscopy to analyze biological materials. *Nat. Protoc.* **2014**, *9*, 1771–1791. [CrossRef]
2. Sabbatini, S.; Conti, C.; Orilisi, G.; Giorgini, E. Infrared spectroscopy as a new tool for studying single living cells: Is there a niche? *Biomed. Spectrosc. Imaging* **2017**, *6*, 85–99. [CrossRef]
3. Magalhães, S.; Goodfellow, B.J.; Nunes, A. FTIR spectroscopy in biomedical research: How to get the most out of its potential. *Appl. Spectrosc. Rev.* **2021**, *56*, 869–907. [CrossRef]
4. Dumas, P.; Miller, L. Biological and Biomedical Applications of Synchrotron Infrared Microspectroscopy. *J. Biol. Phys.* **2003**, *29*, 201–218. [CrossRef]
5. Marcelli, A.; Cricenti, A.; Kwiatek, W.M.; Petibois, C. Biological applications of synchrotron radiation infrared spectromicroscopy. *Biotechnol. Adv.* **2012**, *30*, 1390–1404. [CrossRef] [PubMed]
6. Dumas, P.; Martin, M.C.; Carr, G.L. IR Spectroscopy and Spectromicroscopy with Synchrotron Radiation. In *Synchrotron Light Sources and Free-Electron Lasers*; Jaeschke, E.J., Khan, S., Schneider, J.R., Hastings, J.B., Eds.; Springer Nature Switzerland AG: Cham, Switzerland, 2020.
7. Holman, H.Y.N.; Martin, M.C.; McKinney, W.R. Tracking chemical changes in a live cell: Biomedical applications of SR-FTIR spectromicroscopy. *Spectroscopy* **2003**, *17*, 139–159. [CrossRef]
8. Holman, H.Y.N.; Bechtel, H.A.; Hao, Z.; Martin, M.C. Synchrotron IR Spectromicroscopy: Chemistry of Living Cells. *Anal. Chem.* **2010**, *82*, 8757–8765. [CrossRef]
9. Yu, P.; McKinnon, J.J.; Christensen, C.R.; Christensen, D.A. Using synchrotron-based FTIR microspectroscopy to reveal chemical features of feather protein secondary structure: Comparison with other feed protein sources. *J. Agric. Food Chem.* **2004**, *52*, 7353–7361. [CrossRef] [PubMed]
10. Hughes, C.; Liew, M.; Sachdeva, A.; Bassan, P.; Dumas, P.; Hart, C.A.; Brown, M.D.; Clarke, N.W.; Gardner, P. SR-FTIR spectroscopy of renal epithelial carcinoma side population cells displaying stem cell-like characteristics. *Analyst* **2010**, *135*, 3133–3141. [CrossRef]

11. Mattson, E.C.; Aboualizadeh, E.; Barabas, M.E.; Stucky, C.L.; Hirschmugl, C.J. Opportunities for Live Cell FT-Infrared Imaging: Macromolecule Identification with 2D and 3D Localization. *Int. J. Mol. Sci.* **2013**, *14*, 22753–22781. [CrossRef]
12. Azarfar, G.; Aboualizadeh, E.; Ratti, S.; Olivieri, C.; Norici, A.; Nasse, M.J.; Giordano, M.; Hirschmugl, C.J. Time lapse synchrotron IR chemical imaging for observing the acclimation of a single algal cell to CO_2 treatment. *Sci. Rep.* **2021**, *11*, 13246. [CrossRef]
13. Gault, N.; Rigaud, O.; Poncy, J.L.; Lefaix, J.L. Biochemical Alterations in Human Cells Irradiated with α Particles Delivered by Macro-or Microbeams. *Radiat. Res.* **2007**, *167*, 551–562. [CrossRef]
14. Meade, A.D.; Clarke, C.; Byrne, H.J.; Lyng, F.M. Fourier Transform Infrared Microspectroscopy and Multivariate Methods for Radiobiological Dosimetry. *Radiat. Res.* **2010**, *173*, 225–237. [CrossRef]
15. Meade, A.D.; Howe, O.; Unterreiner, V.; Sockalingum, G.D.; Byrne, H.J.; Lyng, F.M. Vibrational spectroscopy in sensing radiobiological effects: Analyses of targeted and non-targeted effects in human keratinocytes. *Faraday Discuss.* **2016**, *187*, 213–234. [CrossRef] [PubMed]
16. Gianoncelli, A.; Vaccari, L.; Kourousias, G.; Cassese, D.; Bedolla, D.E.; Kenig, S.; Storici, P.; Lazzarino, M.; Kiskinova, M. Soft X ray microscopy radiation damage on fixed cells investigated with synchrotron radiation FT-IR microscopy. *Sci. Rep.* **2015**, *5*, 10250. [CrossRef] [PubMed]
17. Yan, J.; Zhang, F.; Zhang, Q. FTIR Microspectroscopy Probes Particle-Radiation Effect on HCT116 cells (p53+/+, p53−/−). *Radiat. Res.* **2018**, *189*, 156–164. [CrossRef]
18. Ricciardi, V.; Portaccio, M.; Manti, L.; Lepore, M. An FT-IR microspectroscopy ratiometric approach for monitoring X-ray irradiation effects on SH-SY5Y human neuroblastoma cells. *Appl. Sci.* **2020**, *10*, 2974. [CrossRef]
19. Ricciardi, V.; Portaccio, M.; Perna, G.; Lasalvia, M.; Capozzi, V.; Cammarata, F.P.; Pisciotta, P.; Petringa, G.; Delfino, I.; Manti, L.; et al. FT-IR Transflection Micro-spectroscopy Study on Normal Human Breast Cells after Exposure to a Proton Beam. *Appl. Sci.* **2021**, *11*, 540. [CrossRef]
20. Tobin, M.; Puskar, L.; Barber, R.; Harvey, E.; Heraud, P.; Wood, B.; Bambery, K.; Dillon, C.; Munro, K. FTIR spectroscopy of single live cells in aqueous media by synchrotron IR microscopy using microfabricated sample holders. *Vib. Spectrosc.* **2010**, *53*, 34–38. [CrossRef]
21. Vaccari, L.; Birarda, G.; Businaro, L.; Pacor, S.; Grenci, G. Infrared Microspectroscopy of Live Cells in Microfluidic Devices (MDIRMS): Toward a Powerful Label-Free Cell-Based Assay. *Analyst* **2012**, *84*, 4768–4775.
22. Doherty, J.; Raoof, A.; Hussain, A.; Wolna, M.; Cinque, G.; Brown, M.; Gardner, P.; Denbigh, J. Live single cell analysis using synchrotron FTIR microspectroscopy: Development of a simple dynamic flow system for prolonged sample viability. *Analyst* **2019**, *144*, 997–1007. [CrossRef]
23. Chan, K.L.A.; Altharawi, A.; Fale, P.; Song, C.L.; Kazarian, S.G.; Cinque, G.; Untereiner, V.; Sockalingum, G.D. Transmission Fourier Transform Infrared Spectroscopic Imaging, Mapping, and Synchrotron Scanning Microscopy with Zinc Sulfide Hemispheres on Living Mammalian Cells at Sub-Cellular Resolution. *Appl. Spectrosc.* **2020**, *74*, 544–552. [CrossRef]
24. Paganetti, H. *Proton Therapy Physics*; CRC Press, Taylor and Francis Group: Boca Raton, FL, USA, 2012.
25. Luo, L.; Cuaron, J.; Braunstein, L.; Gillespie, E.; Kahn, A.; McCormick, B.; Mah, D.; Chon, B.; Tsai, H.; Powell, S.; et al. Early outcomes of breast cancer patients treated with post-mastectomy uniform scanning proton therapy. *Radiother. Oncol.* **2019**, *132*, 250–256. [CrossRef]
26. Lipiec, E.; Bambery, K.R.; Lekki, J.; Tobin, M.J.; Vogel, C.; Whelan, D.R.; Wood, B.R.; Kwiatek, W.M. SR-FTIR coupled with principal component analysis shows evidence for the cellular bystander effect. *Radiat. Res.* **2015**, *184*, 73–82. [CrossRef]
27. Movasaghi, Z.; Rehman, S.; Rehman, I. Fourier Transform Infrared (FTIR) Spectroscopy of Biological Tissues. *Appl. Spectrosc. Rev.* **2008**, *43*, 134–179. [CrossRef]
28. Yarwood, J.; Shuttleworth, T.; Hasted, J.B.; Nanba, T. A new radiation source for the infrared region. *Nature* **1984**, *312*, 742–744. [CrossRef]
29. Colarusso, P.; Kidder, L.H.; Levin, I.W.; Fraser, J.C.; Arens, J.F.; Lewis, E.N. Infrared Spectroscopic Imaging: From Planetary to Cellular Systems. *Appl. Spectrosc.* **1998**, *52*, 106A–120A. [CrossRef]
30. Carr, G.L. Resolution limits for infrared microspectroscopy explored with synchrotron radiation. *Rev. Sci. Instrum.* **2001**, *72*, 1613–1619. [CrossRef]
31. Quaroni, L.; Zlateva, T. Infrared Spectromicroscopy of Biochemistry in Functional Single Cells. *Analyst* **2011**, *136*, 3219–3232. [CrossRef]
32. Vermorken, A.J.M. *Towards Coordination of Cancer Research in Europe: Results of the 4th EC Biomedical and Health Research Programme*; IOS Press: Amsterdam, The Netherlands, 1994.
33. World Health Organization. Cancer. Available online: www.who.int/news-room/fact-sheets/detail/cancer (accessed on 7 December 2020).
34. Crespo, P. *Optimization of In-Beam Positron Emission Tomography for Monitoring Heavy Ion Tumor Therapy*; WissTech Berichte FZR-444; Helmholtz-Zentrum Dresden Rossendorf: Dresden, Germany, 2005.
35. Nuclear Physics European Collaboration Committee (NuPECC). *Nuclear Physics for Medicine*; NuPECC Report; CRC Press: Boca Raton, FL, USA, 2014.
36. Newhauser, W.D.; Durante, M. Assessing the risk of second malignancies after modern radiotherapy. *Nat. Rev. Cancer* **2011**, *11*, 438–448. [CrossRef]
37. Brahme, A. Recent advances in light ion radiation therapy. *Int. J. Radiation Oncol. Biol. Phys.* **2004**, *58*, 603–616. [CrossRef]

38. Agodi, C.; Calabretta, L.; Cirrone, G.A.P.; Cuttone, G.; Fiorini, F.; Lojacono, P.; Morone, M.C.; Maggiore, M.; De Napoli, M.; Raciti, G.; et al. Heavy Ions Fragmentations Measurements at intermediate energies in hadrontherapy and spatial vehicles shielding. In Proceedings of the IEEE Nuclear Science Symposium Conference Record, Honolulu, HI, USA, 26 October–3 November 2007.
39. Lengauer, C.; Kinzler, K.W.; Vogelstein, B. Genetic instabilities in human cancers. *Nature* **1998**, *396*, 643–649. [CrossRef]
40. Cucinotta, F.A.; Plante, I.; Ponomarev, A.L.; Kim, M.H.Y. Nuclear interactions in heavy ion transport and event-based risk models. *Radiat. Prot. Dosim.* **2011**, *143*, 384–390. [CrossRef]
41. Maalouf, M.; Durante, M.; Foray, N. Biological effects of space radiation on human cells: History, advances and outcomes. *J. Radiat. Res.* **2011**, *52*, 126–146. [CrossRef]
42. Istituto Nazionale di Fisica Nucleare (INFN). Misura e Modellizzazione di Danno Citogenetico Lungo la Curva di Bragg di Ioni Accelerati (MIMO-BRAGG). Available online: http://people.na.infn.it/~{}manti/MIMO-BRAGG/MIMO-BRAGG.xhtml (accessed on 17 December 2020).
43. Nikjoo, S.; Uehara, W.E.; Wilson, M.; Ho, H. Track structure in radiation biology: Theory and applications. *Int. J. Radiat. Biol.* **1998**, *73*, 355–364. [CrossRef]
44. Lipiec, E.; Kowalska, J.; Lekki, J.; Wiechec, A.; KwiateK, K.W. FTIR microspectroscopy in studies of DNA damage induced by proton microbeam in single PC-3 cells. *Acta Phys. Pol. A* **2012**, *121*, 506–509. [CrossRef]
45. Gautam, R.; Vanga, S.; Ariese, F.; Umapathy, S. Review of multidimensional data processing approaches for Raman and infrared spectroscopy. *EPJ Technol. Instrum.* **2015**, *2*, 18. [CrossRef]
46. Lipiec, E.; Bambery, K.R.; Heraud, P.; Hirschmugl, C.; Lekki, J.; Kwiatek, W.M.; Tobin, M.J.; Vogel, C.; Whelan, D.; Wood, B.R. Synchrotron FTIR shows evidence of DNA damage and lipid accumulation in prostate adenocarcinoma PC-3 cells following proton irradiation. *J. Mol. Struct.* **2014**, *1073*, 134–141. [CrossRef]
47. Nasse, M.J.; Walsh, M.J.; Mattson, E.C.; Reininger, R.; Kajdacsy-Balla, A.; Macias, V.; Bhargava, R.; Hirschmugl, C.J. High-Resolution Fourier-transform infrared chemical imaging with multiple synchrotron beams. *Nat. Methods* **2011**, *8*, 413–416. [CrossRef]
48. Rinnan, Å.; Nørgaard, L.; van den Berg, F.; Thygesen, J.; Bro, R.; Balling Engelsen, S. Data Pre-processing. In *Infrared Spectroscopy for Food Quality Analysis and Control*; Sun, D.W., Ed.; Elsevier: Amsterdam, The Netherlands, 2008.
49. Rinnan, A.; den Berg, F.; Engelsen, S.B. Review of the most common pre-processing techniques for near-infrared spectra. *Trends Anal. Chem.* **2009**, *28*, 1201–1222. [CrossRef]
50. Vandeginste, B.G.M.; Massart, D.L.; Buydens, L.M.C.; Jong, S.D.E.; Lewi, P.J.; Smeyers-Verbeke, J. *Handbook of Chemometrics and Qualimetrics, Part B*; Massart, B., Ed.; Elsevier: Amsterdam, The Netherlands, 1998.
51. Delfino, I.; Cavella, S.; Lepore, M. Scattering-based optical techniques for olive oil characterization and quality control. *J. Food Meas. Charact.* **2019**, *13*, 196–212. [CrossRef]
52. Dovbeshko, G.; Gridina, N.Y.; Kruglova, E.B.; Pashchuk, O.P. FTIR Spectroscopy studies of nucleic acid damage. *Talanta* **2000**, *53*, 233–246. [CrossRef]
53. Meade, A.D.; Byrne, H.J.; Lyng, F.M. Spectroscopic and Chemometric Approaches to Radiobiological Analyses. *Mutat. Res. Rev.* **2010**, *704*, 108–114. [CrossRef]
54. Lipiec, E.; Birarda, G.; Kowalska, J.; Lekki, J.; Vaccari, L.; Wiecheć, A.; Wood, B.; Kwiatek, W. A new approach to studying the effects of ionising radiation on single cells using FTIR synchrotron microspectroscopy. *Radiat. Phys. Chem.* **2013**, *93*, 135–141. [CrossRef]
55. Gault, N.; Lefaix, J.L. Infrared microspectroscopic characteristics of radiation-induced apoptosis in human lymphocytes. *Radiat. Res.* **2003**, *160*, 238–250. [CrossRef]
56. Lipiec, E.; Wood, B.R.; Kulik, A.; Kwiatek, W.M.; Dietler, G. Nanoscale investigation into the cellular response of glioblastoma cells exposed to protons. *Anal. Chem.* **2018**, *90*, 7644–7650. [CrossRef]